Available online at www.sciencedirect.com
SCIENCE DIRECT®
Engineering Structures 27 (2005) 514–523
ENGINEERING STRUCTURES
www.elsevier.com/locate/engstruct

A STFT semiactive controller for base isolated buildings with variable stiffness isolation systems

Sriram Narasimhan[a], Satish Nagarajaiah[b,*]

[a]*Department of Civil and Environmental Engineering, Rice University, 6100 S. Main Street, Houston, TX 77005, United States*
[b]*Departments of Civil and Environmental Engineering and Mechanical Engineering and Material Science, Rice University, 6100 S. Main Street, Houston, TX 77005, United States*

Received 20 December 2003; received in revised form 5 November 2004; accepted 15 November 2004
Available online 23 December 2004

Abstract

A new short time Fourier transformation (STFT) control algorithm is developed for reducing the response of base isolated buildings with variable stiffness isolation systems in near fault earthquakes. The central idea of STFT is to break up the signal into small time segments and Fourier analyze each time segment to ascertain the frequencies that exist in it. For each different time a different spectrum is obtained and the totality of these spectra is the time–frequency distribution. STFT is used to determine the energy spectrum and time–frequency distribution of the earthquake excitation signal. Of particular importance is the tracking of the energy of the earthquake excitation corresponding to the fundamental period of the base isolated building. When the energy of the excitation exceeds a predetermined threshold value the STFT controller varies the stiffness of the isolation system smoothly between minimum and maximum values to achieve response reduction. The main reason for the response reduction is the variation of the fundamental frequency of the base isolated building. Additionally, the STFT control algorithm ensures passivity and energy dissipation during the smooth variation of the stiffness. The STFT algorithm is implemented analytically on a five-story base isolated reinforced concrete building with linear elastomeric isolation bearings and a variable stiffness system located at the isolation level. Several recent near fault earthquakes are considered. It is shown that the controller is effective in reducing the base displacements and interstory drifts without increasing floor accelerations. The novelty of the STFT controller lies in its effective variation of stiffness only a few times to achieve response reduction, which makes it suitable for practical implementation.

Keywords: Semiactive control; STFT; Variable stiffness; Base isolated buildings

1. Introduction

The application of semiactive variable stiffness and damping devices has been investigated and demonstrated to be effective by many researchers (e.g., [16]). Passive structural control methods such as base isolation [3], supplemental fluid dampers, tuned mass dampers are widely accepted. For the case of base isolation systems with sliding or elastomeric bearings, the addition of passive damping at the isolation level to reduce the base displacements in near fault earthquakes may lead to increased interstory drifts and floor accelerations [7,4]. An attractive alternative is the use of semiactive systems. The primary goal of this study is to develop a new control algorithm for the semiactive variable stiffness (SAIVS) system to achieve response reductions in base isolated buildings subjected to near fault earthquakes.

Semiactive control of linear and nonlinear structures using novel devices such as variable stiffness systems, magnetorheological (MR) dampers and electrorheological (ER) dampers has gained significant attention in recent years [5–7,12–15,17,20,21]. The effectiveness of structural control strategies and different control algorithms has been demonstrated, by many researchers, experimentally and

* Corresponding address: George R. Brown School of Engineering, Rice University, MS 318, 6100 Main Street, Houston, TX 77005, United States. Tel.: +1 713 348 6207; fax: +1 713 348 5268.
E-mail addresses: nsriram@rice.edu (S. Narasimhan), nagaraja@rice.edu (S. Nagarajaiah).

0141-0296/$ - see front matter © 2004 Elsevier Ltd. All rights reserved.
doi:10.1016/j.engstruct.2004.11.010

analytically [16]. The primary advantage of variable stiffness systems is their ability to avoid resonance [5,10]. The active variable stiffness system [5] has performed successfully in several earthquakes; however, the on–off device can switch stiffness between on–off states and may in some cases lead to increased accelerations. To overcome the limitation of abrupt switching, a new semiactive independently variable stiffness (SAIVS) device has been developed [10,9]. The SAIVS device is capable of switching the stiffness smoothly. The control algorithm proposed by Kobori et al. [5] is based on estimation of the response in each stiffness state and selection of the state which results in the least response. The controller developed by Yang et al. [19] is a sliding mode controller. The resetting algorithms [2,18] are effective primarily due to energy dissipation with constant stiffness. The tuned interaction damper [22] is based on Lyapunov theory. The aforementioned studies do not estimate the energy spectrum and time–frequency distribution of the ground excitation needed for developing a variable stiffness control strategy for response reduction.

In this paper the use of short time Fourier transformation (STFT) to track the energy spectrum and the time–frequency distribution of the earthquake for response control is proposed. Of particular importance is the proposed tracking of energy of the earthquake excitation, corresponding to the fundamental period of the base isolated building, used in developing the variable stiffness control algorithm. When the energy of the excitation exceeds a certain threshold value the STFT controller varies the stiffness of the isolation system smoothly between minimum and maximum values to achieve response reduction. The STFT algorithm is implemented analytically on a five-story base isolated reinforced concrete building with linear elastomeric isolation bearings and a variable stiffness system located at the isolation level. Several recent near fault earthquakes are considered. It is shown that the controller is effective in reducing the base displacements and interstory drifts without increasing floor accelerations.

2. Structure with a variable stiffness system: formulation

The equations of motion for the base isolated structure are developed on the basis of a three-dimensional formulation consisting of two lateral degrees of freedom and one rotational degree of freedom at the center of mass of each floor and the base. The state space equations for the superstructure and the base are formulated as follows:

$$\dot{\mathbf{x}}(t) = \mathbf{A}\mathbf{x}(t) + \mathbf{B}\mathbf{u}(t) + \mathbf{E}\mathbf{a}_g(t) = \mathbf{g}(\mathbf{x}, \mathbf{u}, \mathbf{a}_g) \tag{1}$$

where $\mathbf{X} = \{\mathbf{U}^T \quad \mathbf{U}_b^T \quad \dot{\mathbf{U}}^T \quad \dot{\mathbf{U}}_b^T\}^T$,

$$\mathbf{A} = \begin{bmatrix} \mathbf{0} & \mathbf{I} \\ -\overline{\mathbf{M}}^{-1}\overline{\mathbf{K}} & -\overline{\mathbf{M}}^{-1}\overline{\mathbf{C}} \end{bmatrix}, \qquad \mathbf{B} = \begin{bmatrix} \mathbf{0} \\ -\overline{\mathbf{M}}^{-1} \end{bmatrix},$$

$$\mathbf{E} = \begin{bmatrix} \mathbf{0} \\ -\overline{\mathbf{M}}^{-1} \begin{Bmatrix} \mathbf{MR} \\ \mathbf{R}^T\mathbf{MR} + \mathbf{M}_b \end{Bmatrix} \end{bmatrix},$$

$$\overline{\mathbf{M}} = \begin{bmatrix} \mathbf{M} & \mathbf{MR} \\ \mathbf{R}^T\mathbf{M} & \mathbf{R}^T\mathbf{MR} + \mathbf{M}_b \end{bmatrix}, \qquad \overline{\mathbf{C}} = \begin{bmatrix} \mathbf{C} & \mathbf{0} \\ \mathbf{0} & \mathbf{C}_b \end{bmatrix},$$

$$\overline{\mathbf{K}} = \begin{bmatrix} \mathbf{K} & \mathbf{0} \\ \mathbf{0} & \mathbf{K}_b \end{bmatrix}, \qquad \mathbf{u} = \begin{bmatrix} \mathbf{0} \\ \mathbf{f}_d \end{bmatrix}.$$

In the above equations, **A**, **B** and **E** are system matrices. **M** is the superstructure mass matrix, **C** is the superstructure damping matrix in the fixed base case, **K** is the superstructure stiffness matrix in the fixed base case, $\mathbf{M}_b$ is the mass of the rigid base, $\mathbf{C}_b$ is the damping of isolation system, $\mathbf{K}_b$ is the total stiffness of elastic isolation elements and $\mathbf{f}_d$ is the vector of force from the control devices. **R** is the matrix of earthquake influence coefficients consisting of zeros corresponding to rotational degree of freedom and ones corresponding to the two lateral degrees of freedom. Furthermore, $\ddot{\mathbf{U}}$, $\dot{\mathbf{U}}$ and **U** represent the floor acceleration, velocity and displacement vectors relative to the base, $\ddot{\mathbf{U}}_b$ is the base acceleration relative to the ground and $\mathbf{a}_g$ is the ground acceleration in two perpendicular directions (x and y). The evaluation and measured output equations are

$$\dot{\mathbf{x}} = \mathbf{A}\mathbf{x} + \mathbf{B}\mathbf{u} + \mathbf{E}\mathbf{a}_g \tag{2}$$

$$\mathbf{z} = \mathbf{C}\mathbf{x} + \mathbf{D}\mathbf{u} \tag{3}$$

$$\mathbf{y}_m = \mathbf{C}_m\mathbf{x} + \mathbf{D}_m\mathbf{u} + \mathbf{E}\mathbf{a}_g + \mathbf{v} \tag{4}$$

where **z** is the evaluation output vector which is obtained by choosing the appropriate mapping matrices, **C** and **D**. The evaluation output vector, **z**, consists of the base displacement, floor accelerations and interstory drifts. $\mathbf{y}_m$ is the measurement vector consisting of the relative velocity at the device connection points, force in the devices and ground acceleration. These can be obtained by choosing appropriate mapping matrices $\mathbf{C}_m$ and $\mathbf{D}_m$. **v** is the measurement noise vector which is assumed to be white noise. The **E** matrix is chosen to include the measured ground acceleration.

2.1. Sensor model

The sensors are modeled as follows:

$$\dot{\mathbf{X}}^s = \mathbf{g}_1(\mathbf{X}^s, \mathbf{y}_m, \mathbf{f}_d, t) \tag{5}$$

$$\mathbf{y}_s = \mathbf{g}_2(\mathbf{X}^s, \mathbf{y}_m, \mathbf{f}_d, \mathbf{v}, t) \tag{6}$$

where $\mathbf{X}^s$ are the states of the sensor, **v** is the measurement noise vector, $\mathbf{f}_d$ is the vector of device forces and $\mathbf{y}_s$ is the output of the sensor in volts. $\mathbf{y}_m$ consists of the relative velocity at the location of the devices that is needed for feedback into the controller and ground accelerations.

2.2. The control algorithm

The control algorithm is implemented in the discrete domain as follows:

$$\mathbf{X}^c_{k+1} = \mathbf{g}_3(\mathbf{X}^c_k, \mathbf{y}_{ks}, k) \quad (7)$$

$$\mathbf{I}_{dk} = \mathbf{g}_4(\mathbf{X}^c_k, \mathbf{y}_{ks}, k) \quad (8)$$

where $\mathbf{X}^c_k$ is the discrete state vector of the controller at time $t_k = k\Delta t$, $\mathbf{y}_{ns}$ is the discretized sensor model output and $\mathbf{I}_{dk}$ is the discrete control command from the control algorithm.

2.3. Control devices

The control device is interfaced with the building model as follows:

$$\mathbf{f}_d = \mathbf{g}_5(\mathbf{y}_d, \mathbf{I}_d, t) \quad (9)$$

where $\mathbf{y}_d$ consists of displacement and velocity at the device connection points. Eq. (1) is solved using the unconditionally stable Newmark's constant average acceleration method, which can also be derived from the trapezoidal rule given by

$$\mathbf{x}_{k+1} = \mathbf{x}_k + \frac{\Delta t}{2}(\mathbf{g}_k + \mathbf{g}_{k+1}) \quad (10)$$

where $\mathbf{g}_{k+1} = \mathbf{g}(\mathbf{x}_{k+1}, \mathbf{u}_{k+1}, \mathbf{a}_{g_{(k+1)}})$. The state equations defined above along with the device model form a time-variant system and hence an implicit method that needs iteration is used [11].

2.4. The semiactive variable stiffness device (SAIVS)

The semiactive variable stiffness device (SAIVS) is capable of providing smooth stiffness variation along the x or y direction depending on its orientation. In the current study the earthquake excitation is considered in the x direction only (uniaxial case). Hence, the SAIVS device is oriented to provide variable stiffness in the x direction only. The analytical model for a single SAIVS device is shown in Fig. 1. It consists of four sets of spring elements arranged in a rhombus configuration as shown. Each of the four spring elements in the device is located at an angle, θ to the horizontal. The four springs are connected to joints 1–4 as shown in Fig. 1. Joint 1 is fixed in the x direction and can be positioned at any desired position in the y direction by a linear electromechanical actuator and controller. Joint 2 is free to move in both the x and y directions. Joints 3 and 4 are free to move in the x direction only. The ends of the guide rail, on which joint 2 moves, are attached to the base slab. The ends of the guide rail, on which joints 3 and 4 move, are attached to the ground. The electromechanical actuator is fixed to the ground and can actuate in the y direction, thus moving joint 1 to the required position. The force developed at any time in the device for a specific position is given by

$$f_{dx}(t) = \{k_e \cos^2\theta(t)\} y_{dx}(t) \quad (11)$$

where $y_{dx}(t)$ is the relative displacement (between the base and ground) at joint 2 in the x direction, k_e is the stiffness of a single spring, $\theta(t)$ is the time varying angle of the spring elements with the horizontal for any given device position.

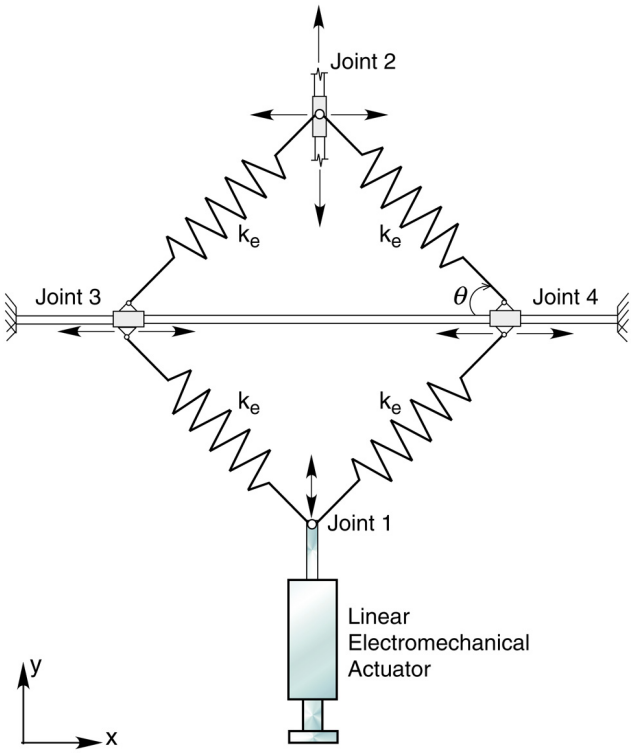

Fig. 1. The analytical model of the SAIVS device.

The angle of the spring is a function of the controller output command voltage, I_{dx}, to the linear actuator of the device as in Eq. (8). The device generates a certain f_{dx} (Eq. (11)) for a particular angle. For example, when $\theta = 20.28°$, $k_{\max} = 61{,}600$ kN/m (passive on) and when $\theta = 67.2°$, $k_{\min} = 10{,}512$ kN/m (passive off). For intermediate θ, the stiffness, k_i, varies between $k_{\max}$ and $k_{\min}$ (refer to Fig. 4). Although the device is linear, as the device angle is changed, stiffness varies, resulting in hysteretic behavior leading to additional energy dissipation.

3. Short time Fourier transformation (STFT)

Short time Fourier transformation (STFT) is the most widely used method for studying non-stationary signals. The basic idea of STFT is to break up the signal into small time segments and Fourier analyze each time segment to ascertain the frequencies that exist in that segment. For each different time a different spectrum is obtained and the totality of such a spectrum indicates the time–frequency distribution. The STFT procedure is ideal in many respects. It is well defined, on the basis of reasonable physical principles, and for many signals and situations it gives an excellent time–frequency structure consistent with intuition [1].

To study the properties of the signal, say a_{gx}, at time t, the signal at that time is emphasized and the signal at other times is suppressed. This is achieved by multiplying the signal by a window function, $h(t)$, centered at t, to produce a modified

signal,

$$\hat{a}_{g_{xt}}(\tau) = a_{gx}(\tau)h(\tau - t). \tag{12}$$

The modified signal is a function of two times, the fixed time, t, that is of interest, and the running time, τ. The window function, h is chosen to leave the signal more or less unaltered around the time t but to suppress the signals for times distant from the time of interest. The resulting short time Fourier transform reflecting the distribution of frequency around that time is given by

$$A_t(\omega) = \frac{1}{\sqrt{2\pi}} \int \mathrm{e}^{-j\omega\tau} \hat{a}_{g_{xt}}(\tau)\mathrm{d}\tau \tag{13}$$

$$= \frac{1}{\sqrt{2\pi}} \int \mathrm{e}^{-j\omega\tau} a_{g_{xt}}(\tau)h(\tau - t)\mathrm{d}\tau. \tag{14}$$

The energy density spectrum at time t is therefore

$$P_{SP}(t, \omega) = |A_t(\omega)|^2 = \left| \frac{1}{\sqrt{2\pi}} \int \mathrm{e}^{-j\omega\tau} a_{g_{xt}}(\tau)h(\tau - t)\mathrm{d}\tau \right|^2. \tag{15}$$

For each different time a different spectrum is obtained and the totality of these spectra is the time–frequency distribution, $\mathbf{P}_{SP}$, called the "spectrogram". The spectrogram for any signal results in a matrix $\mathbf{P}_{SP}$ of size $m \times n$ where m is the number of frequency intervals and n the number of time steps. The power computed on a linear scale is converted to a logarithmic scale in decibels (dB) for the purposes of algorithm implementation.

4. The STFT control algorithm

For simplicity the STFT control algorithm is implemented only in the x direction; however, it can easily be extended to both x and y directions in general. Such an assumption is deemed appropriate in the current study since the excitation is considered only in the x direction (uniaxial case). The control block diagram is shown in Fig. 2. At time $t = 0$ the stiffness value of the SAIVS device is set to its maximum, $k_{\max}$. The control algorithm is as follows:

1. A moving window (advanced at every time step) of n time steps of signal is chosen. At any time t_k the signal is multiplied with the 'Hanning' window function, h as in Eq. (12).
2. The energy density spectrum at t_k is computed using the STFT in discrete form resulting in a vector $\mathbf{P}_{SP}^{t_k}$ of size $m \times 1$.
3. From the vector of the energy density spectrum, $\mathbf{P}_{SP}^{t_k}$, the scalar $P_{f\,\max}^{t_k}$ is selected, corresponding to $f_{\max}$ which is the fundamental frequency at $k_{\max}$.
4. One of the following steps is implemented next: (i) step 5 is implemented if the current stiffness state is $k_{\max}$ and smooth stiffness variation is continued until $k_{\min}$ is reached; or (ii) step 6 is implemented if the current stiffness state is $k_{\min}$ and smooth stiffness variation is continued until $k_{\max}$ is reached; or (iii) the algorithm is restarted at step 1.
5. The smooth stiffness variation from $k_{\max}$ to $k_{\min}$ begins at the instant, t_k^{uc}, when $P_{f\,\max}^{t_k}$ is increasing and exceeds (termed upcrossing at t_k^{uc}) a predetermined threshold value, ς. A smoothing function, $\lambda^+ = 2/(1 + \mathrm{e}^{+\alpha\tau_k^l})$ is used to vary the stiffness from $k_{\max}$ to $k_{\min}$, where α is a constant (a value of 4 is chosen for the current study) and τ_k^l is the discrete elapsed local time beginning at the upcrossing instant t_k^{uc}. Once $k_{\min}$ is reached, the local time τ_k^l is continued into step 6, which always follows step 5.
6. The smooth stiffness variation from $k_{\min}$ to $k_{\max}$ begins when the two conditions (i) $f_{dxk}\dot{y}_{dxk} > 0$ and (ii) $\tau_k^l \geq \delta$ are satisfied, where f_{dxk} is the force in the SAIVS device, $\dot{y}_{dxk}$ is the relative velocity at the device location, τ_k^l is the discrete elapsed local time and δ is a constant. The first condition ($f_{dxk}\dot{y}_{dxk} > 0$) is checked before the stiffness is varied from $k_{\min}$ to $k_{\max}$, in order to ensure that the stiffness change is always dissipative in nature. The second condition ($\tau_k^l \geq \delta$) is checked to ensure adequate time for the stiffness recovery from $k_{\min}$ to $k_{\max}$ and to allow for the smooth variation of the stiffness. The stiffness is varied from $k_{\min}$ to $k_{\max}$ using the smoothing function $\lambda^- = 2/(1 + \mathrm{e}^{-\alpha\tau_k^l})$. Once $k_{\max}$ is reached, the local time τ_k^l is reset to zero.

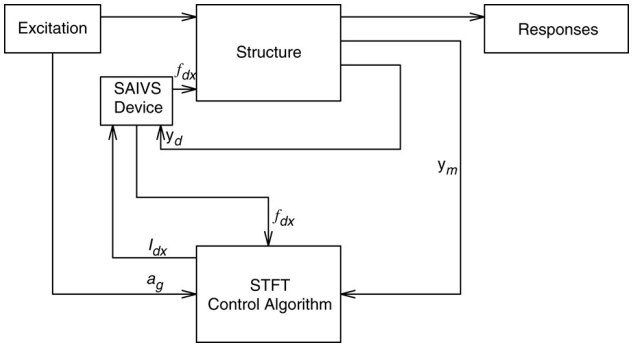

Fig. 2. The block diagram for control implementation.

5. Application of the STFT controller: a numerical example

The structure considered is a symmetric base isolated five-story building of length $L = 55$ m and width $W = 55$ m. The superstructure bracing is located at the building perimeter. Metal decking and a grid of beams support all concrete floor slabs. The steel superstructure is supported on a reinforced concrete base slab, which is integral to concrete beams below, and drop panels below each column location. The isolators are connected between these drop panels and the footings below as shown in Fig. 3. The superstructure is modeled as a three-dimensional linear elastic system. The superstructure members, such as the beam, column, bracing and floor slab, are modeled in detail. Floor slabs

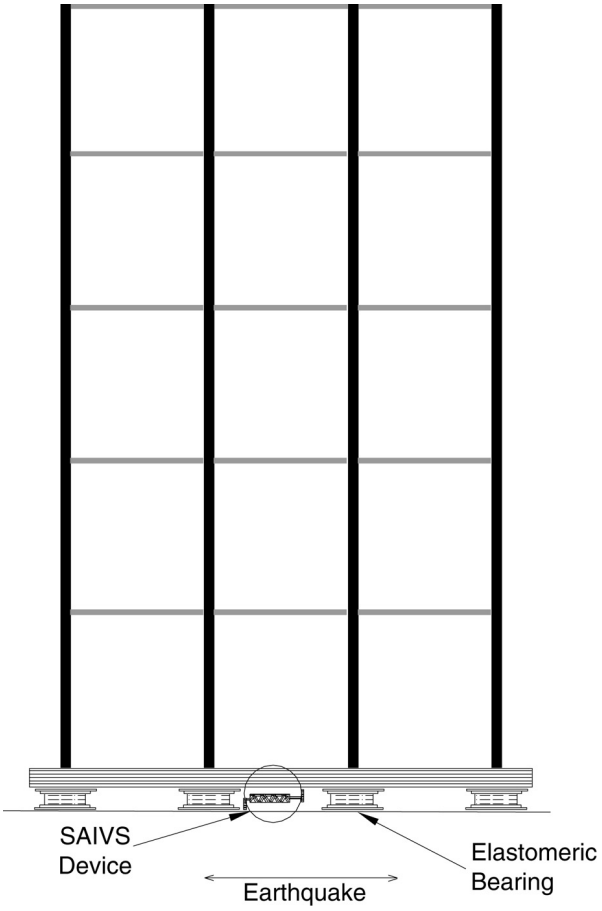

Fig. 3. A base isolated building with a variable stiffness isolation system.

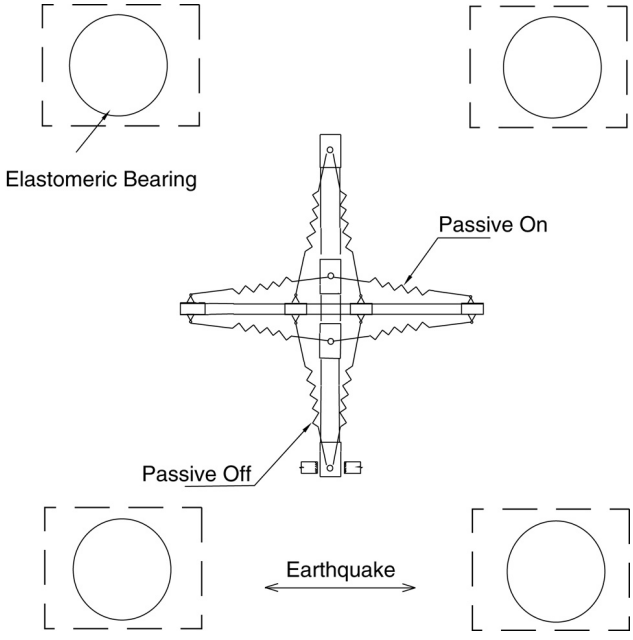

Fig. 4. Detail of the SAIVS device with four surrounding elastomeric bearings.

and the base are assumed to be rigid in the plane. The superstructure and the base are modeled using three master

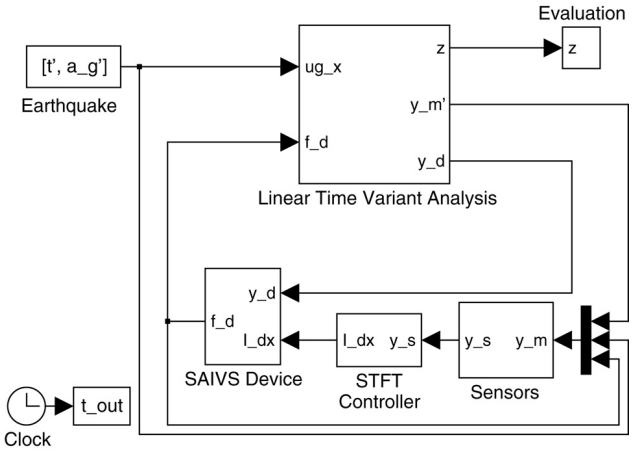

Fig. 5. The Simulink block diagram for simulation.

degrees of freedom (DOF) per floor at the center of mass. The combined model of the superstructure (15 DOF) and isolation system (3 DOF) consists of 18 degrees of freedom. The superstructure damping ratio is assumed to be 5% in all fixed base modes and 2% critical for the elastomeric bearings. The first nine modes are used for modeling the superstructure. The computed periods T_n for the nine modes in the fixed base condition (along the three DOF) are 0.73, 0.57, 0.43, 0.29, 0.23, 0.17, 0.14, 0.12 and 0.10 s. The eccentricities at all floors are chosen to be zero. The total weight of the structure is 142,575 kN. There are 61 linear elastomeric bearings each with a stiffness of 1435.5 kN/m (total stiffness of 87,565 kN/m). The variable stiffness device is assumed to be connected at the center of mass of the base only in the x direction, as shown in Figs. 3 and 4 (the restoring force is assumed to be coincident with the center of mass). The SAIVS device shown in Fig. 4 has been magnified for clarity. The stiffness $k_e = 70{,}000$ kN/m of the SAIVS device is chosen so as to provide a fundamental period of 2 s ($f_{\max} = 0.5$ Hz) in the passive on case ($k_{\max} = 61{,}600$ kN/m) and 2.5 s ($f_{\min} = 0.4$ Hz) in the passive off case ($k_{\min} = 10{,}512$ kN/m). The equations of motion are solved using a constant average acceleration method inside the S function block named Linear Time Variant Analysis as shown in the Simulink block diagram in Fig. 5. The STFT computation is performed using the standard blocks available within the Simulink toolbox [8].

The structure considered here is excited by the following set of near fault ground motions in the uniaxial x direction as shown in Figs. 3 and 4:

- *Newhall*—the fault normal Newhall component of the 1994 Northridge earthquake, with a peak ground acceleration of $0.736g$;
- *Sylmar*—the fault parallel component of the 1994 Northridge earthquake recorded in Sylmar county, with a peak ground acceleration of $0.605g$;
- *Kobe*—the East–West component of the Kobe earthquake (JMA), with a peak ground acceleration of $0.631g$.

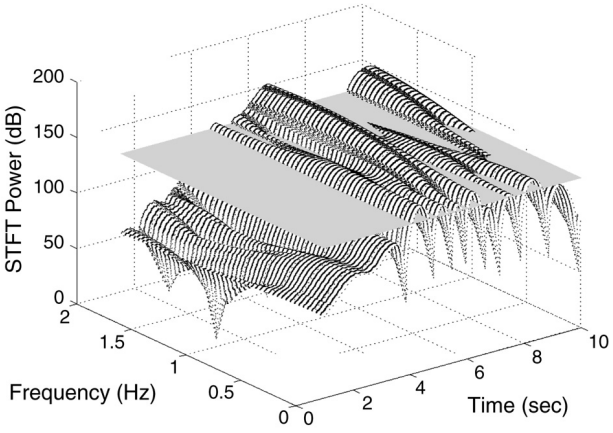

Fig. 6. The STFT spectrogram for the Newhall earthquake.

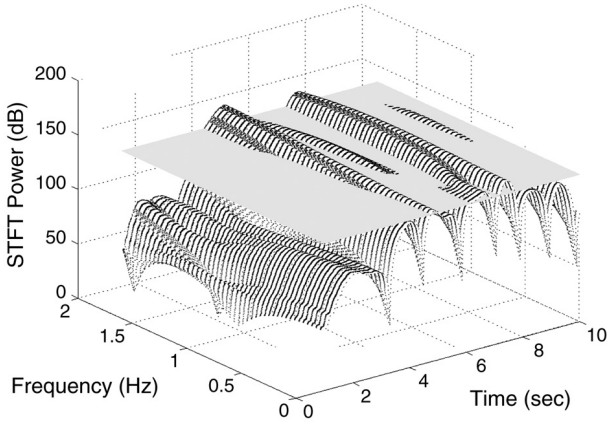

Fig. 7. The STFT spectrogram for the Sylmar earthquake.

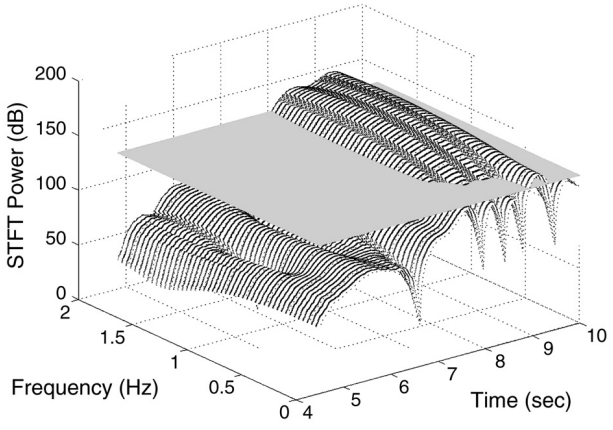

Fig. 8. The STFT spectrogram for the Kobe earthquake.

5.1. STFT spectrograms of earthquakes

The spectrograms for three excitations, Newhall, Sylmar and Kobe, are shown in Figs. 6–8 with time plotted on the x axis, frequency on the y axis and the STFT power (in decibels, dB) on the z axis. Also shown in these figures is a threshold level that intersects the surface of the STFT spectrogram at all frequencies. The value of the threshold

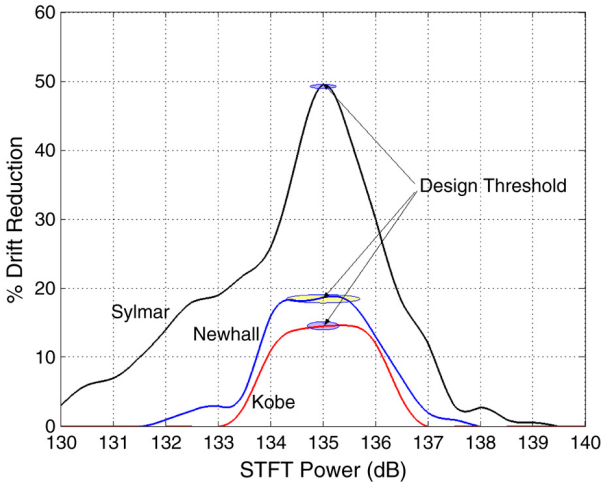

Fig. 9. Determination of the threshold, ς.

parameter, ς, described in the earlier sections is determined on the basis of a parametric study of variables in the algorithm. This parametric study is conducted for the set ground motions considered, namely, Newhall, Sylmar and Kobe. For each windowing operation, 256 earthquake data points are taken and zero-padded to length 2048. To this zero-padded data, a Hanning window of time duration $\Delta t = 10.24$ s (frequency bandwidth of $\Delta_\omega = 0.098$ Hz) is applied for STFT computation. The results of this study are shown in Fig. 9. The results are plotted in terms of the percentage reduction of story drifts achieved for various values of ς that result in positive drift reductions. On the basis of the performance of the threshold level ς that is optimal over the three ground excitations, $\varsigma = 135$ dB is chosen as the design value for simulations.

5.2. Structural responses

Fig. 10 shows the base displacement responses of the base isolated building due to Newhall, Sylmar and Kobe earthquake excitations in the uniaxial direction. Three cases considered are (i) passive off, where the SAIVS device develops its minimum stiffness, (ii) passive on, where the SAIVS device develops its maximum stiffness, and (iii) controlled, where the new STFT algorithm described in the earlier sections is implemented. The stiffness variation time histories are shown in Fig. 11 for the three excitations. Also shown in Fig. 11 is a slice of the STFT spectrogram at 2 s (the fundamental period of the passive on case) as a function of time. In the controlled case when the magnitude of the STFT exceeds the threshold value during upcrossing, the stiffness is varied smoothly from the passive on to the passive off position and, after the passivity and elapsed time considerations are satisfied, it is varied smoothly from the passive off to the passive on position. The threshold level is fixed at 135 dB for all three excitations and the parameter $\delta = 0.25$ s $(T_n/8)$ is chosen. The parameter is $\alpha = 4.0$ for the current study. The $\pm$ sign for α is determined by

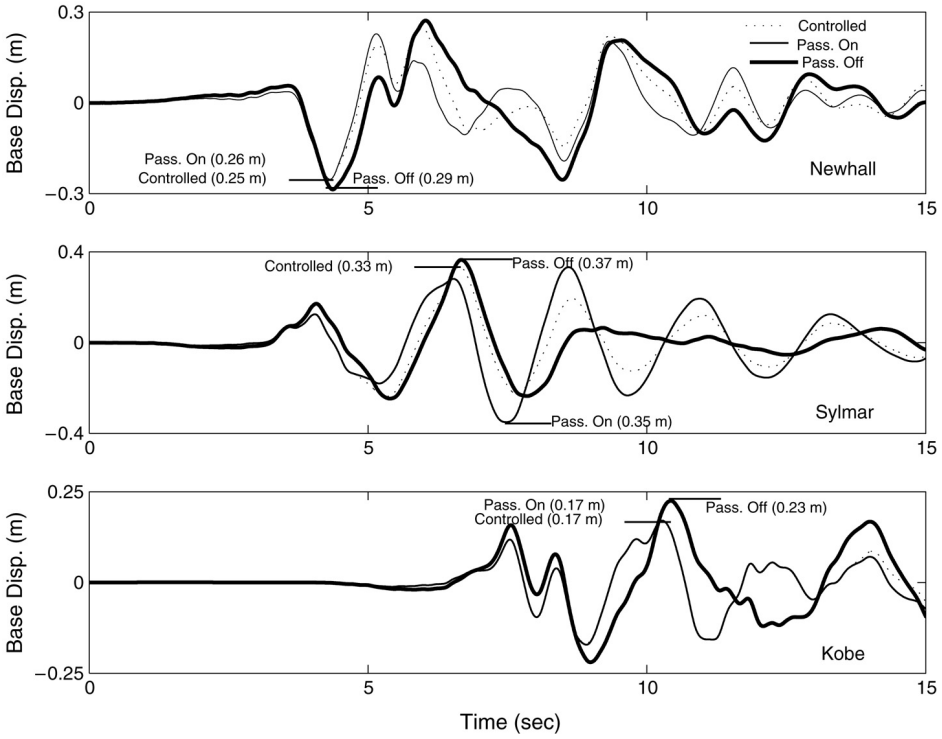

Fig. 10. Base displacement responses for Newhall, Sylmar and Kobe excitations.

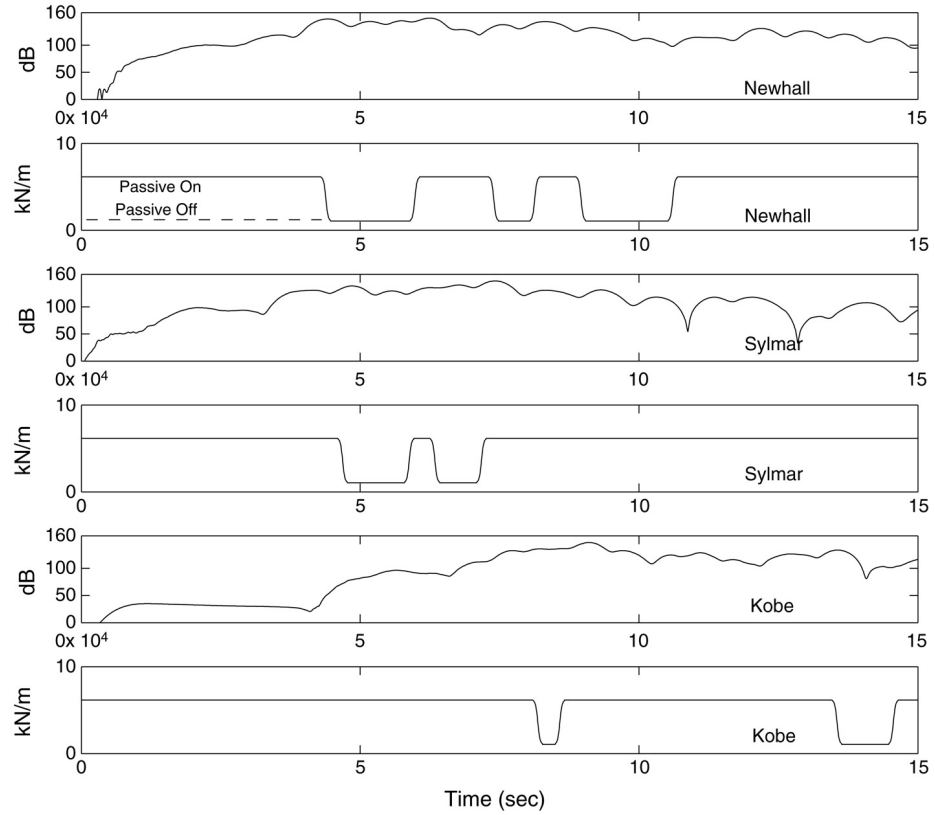

Fig. 11. STFT power and stiffness time histories for Newhall, Sylmar and Kobe excitations.

the direction of switching: from maximum to minimum or vice versa. Fig. 12 shows the peak base displacement as a function of peak ground acceleration in passive on, passive off and controlled cases for the three earthquakes. From the results we can see that the reductions in the peak base displacements for the controlled case compared to the passive off case are 14% for Newhall, 11% for Sylmar and 26% for Kobe. The corresponding reductions for the controlled case compared to the passive on case are 4% and 6% for Newhall and Sylmar respectively. The peak base displacements for Kobe excitation are the same as in the passive on case. The controlled case reduces the peak base displacement response in all three earthquakes. In particular, in the case of Newhall and Sylmar with peak base displacement greater than 0.25 m, the controlled case reduces the response further than the passive on case. It can be observed from Fig. 10 that the controlled case remains bounded between the passive on and passive off cases. Also, it is evident in Fig. 10 that the stiffness and frequency vary from passive on to passive off or vice versa to avoid peak displacement response during the peak STFT power in Newhall and Sylmar earthquakes. In the case of the Kobe earthquake the controlled case remains at the passive on state most of the time since the least displacement response occurs in that state. Fig. 13 shows the peak interstory drifts at various floor levels for all three excitations considered. From Fig. 13 it is evident that the story drifts are substantially reduced for the controlled case as compared to the passive on case in all three earthquakes for all the floors. Maximum drift reductions in the controlled case for the Newhall, Sylmar and Kobe earthquakes are 18%, 49% and 15%, respectively, when compared to the passive on case, and nearly the same when compared to the passive off case. Comparing Figs. 12 and 13, it is evident that the greatest reduction in the interstory drifts (49%) is achieved where the magnitude of the base displacement is the highest (Sylmar excitation). It is also worth noting from Figs. 12 and 13 that in the passive on case the base displacements are smaller due to a stiffer isolation system; however, the interstory drifts are larger. In contrast, in the passive off case the base displacements are larger; however, the interstory drifts are smaller. In the controlled case both the base displacements and interstory drifts are smaller, which clearly indicates the advantage of the new STFT controller. The peak floor accelerations shown in Fig. 14 are maintained at the same levels as in the passive off case. Only in the case of Newhall is the first floor acceleration for the controlled case reduced by nearly 10%. This shows that the STFT controller with smooth stiffness variation does not introduce additional accelerations in the lower stories as compared to on–off stiffness switching algorithms developed by other researchers [19,14]. The force–displacement plots are shown in Fig. 15. The magnitude of the SAIVS force is normalized by the total weight of the structure. The stiffness variation is clearly evident in Fig. 15. It is the stiffness or frequency variation which leads to drift response reduction.

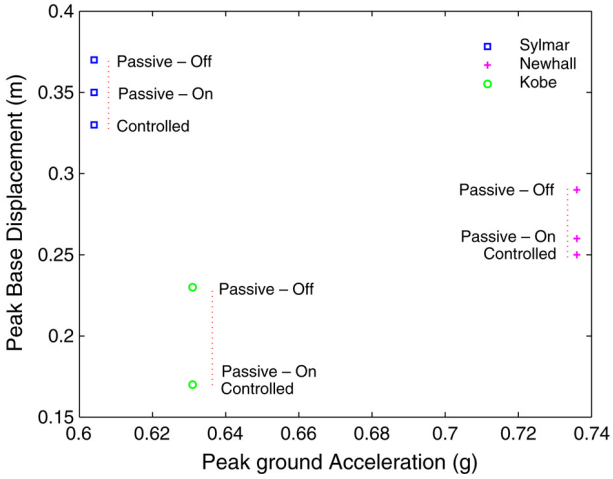

Fig. 12. Base displacement responses for Newhall, Sylmar and Kobe excitations.

This can be inferred from the response in Kobe—the drift response is reduced by nearly 15% with stiffness variation of the isolation system and with minimal additional energy dissipation in the isolation system (see Fig. 15(c)).

The estimated time delay in the online implementation of this algorithm is investigated through simulations; only a summary of the results is reported here for brevity. The time delay for STFT implementation is nearly five milliseconds (ms). However, for evaluation purposes, delays of 25 and 50 ms are introduced and the simulations are performed. The greatest effect of the time delay is on the magnitude of the base displacement. For the case of the Kobe earthquake, on introducing a delay of 50 ms, the base displacements increased by 5% and by 3.7% for a delay of 25 ms, compared to the baseline case of 5 ms. By comparison, for a 50 ms delay, the base displacements increased by 2% for Sylmar and 2.27% for Newhall. Similarly, the increases in the base displacement for 25 ms delay for Sylmar and Newhall are 1.5% and 1.88% respectively. The effect of time delay on interstory drifts and accelerations is less than 2% for 50 ms delay and less than 1.3% for 25 ms delay for all three earthquakes.

6. Conclusions

A new variable stiffness control algorithm based on STFT has been developed and shown to be effective in reducing the response of base isolated buildings in near fault earthquakes. The variation of stiffness is based on tracking the energy of the earthquake excitation at the fundamental period. In base isolated buildings with stiffer isolation systems, generally the base displacements are smaller and interstory drifts are larger. Exactly the opposite response results in cases with softer isolation systems. However, in the controlled case both the base displacement and interstory drifts are reduced. Simulated results show that the greatest

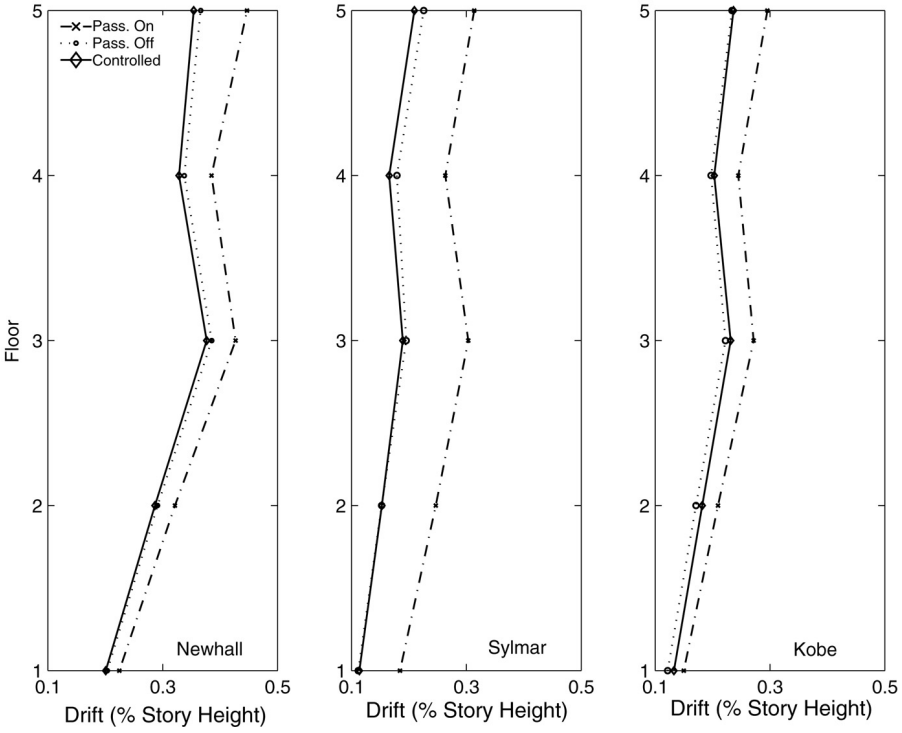

Fig. 13. Story drifts for Newhall, Sylmar and Kobe excitations.

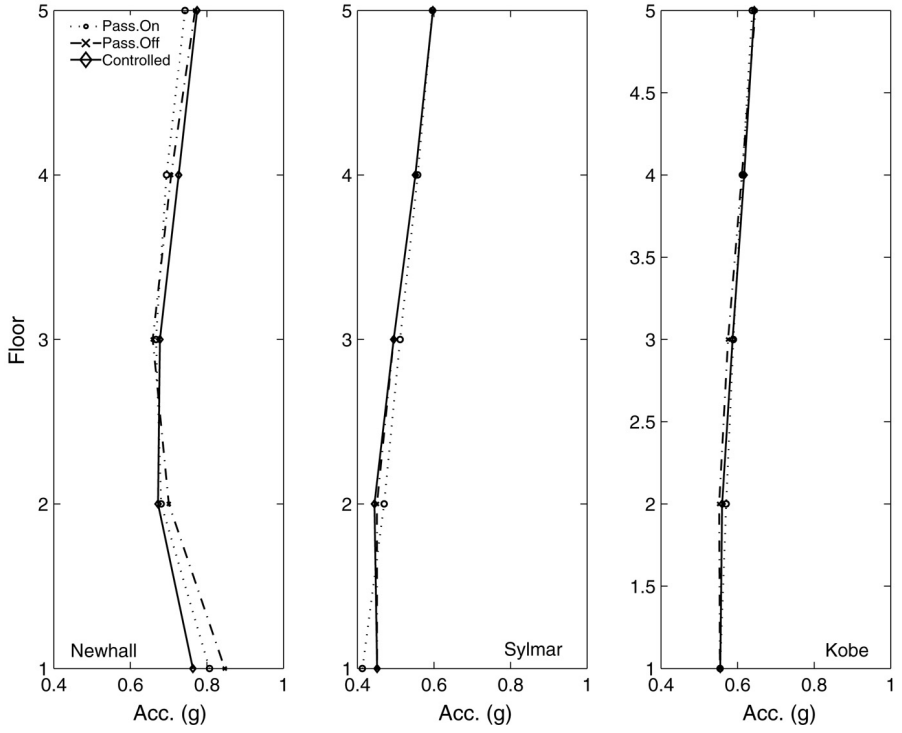

Fig. 14. Peak floor accelerations for Newhall, Sylmar and Kobe excitations.

reduction in interstory drifts occurs when the magnitude of the base displacement is the largest. No increase in acceleration in the lower stories occurs due to the few smooth stiffness variations as compared to the increase in acceleration in the lower stories observed in on–off stiffness algorithms with rapid and abrupt switching. This study also shows that algorithms based on the time–frequency content of the ground excitation hold significant promise

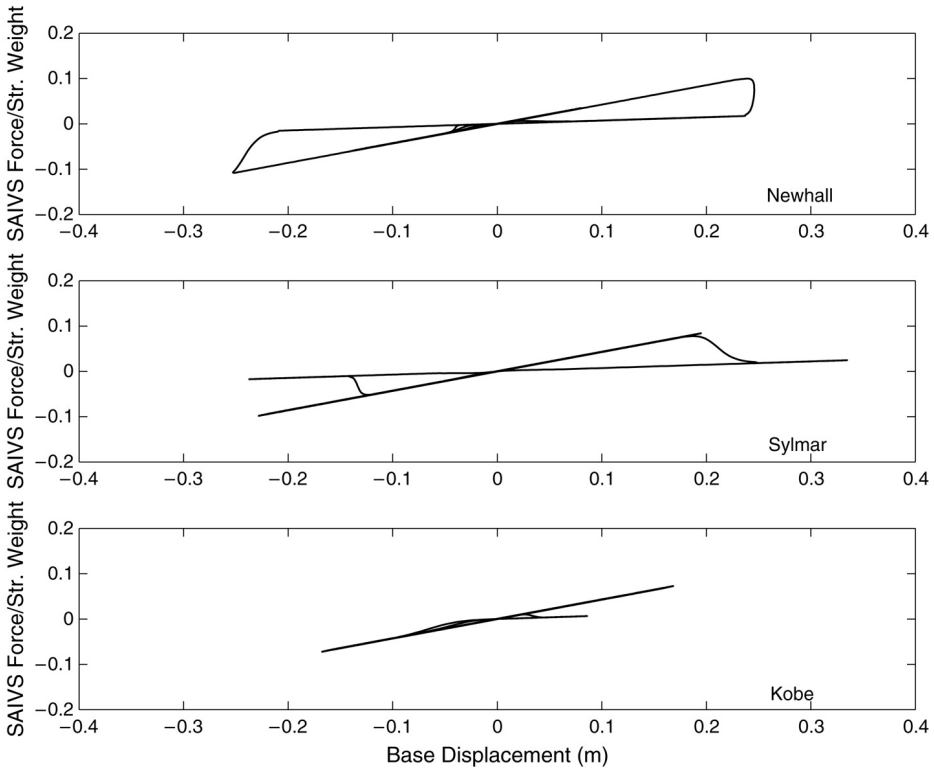

Fig. 15. Force–displacement loops of variable stiffness devices for Newhall, Sylmar and Kobe excitations.

for use with variable stiffness devices in base isolation applications.

Acknowledgements

Funding provided by the National Science Foundation, CAREER Award 99-96290, is gratefully acknowledged.

References

[1] Cohen L. Time–frequency analysis. NJ: Prentice-Hall; 1995.
[2] Jabbari F, Bobrow JE. Vibration suppression with resettable device. J Struct Eng, ASCE 2002;128(9):916–24.
[3] Kelly J. State-of-the-art and state-of-the-practice in base isolation. In: ATC-17-1 seminar on seismic isolation, passive energy dissipation and active control. 1993.
[4] Kelly J. The role of damping in seismic isolation. Earthq Eng Struct Dyn 1999;28:3–20.
[5] Kobori T, Takahashi M, Nasu T, Niwa N, Ogasawara K. Seismic response controlled structure with active variable stiffness system. Earthq Eng Struct Dyn 1993;22:925–41.
[6] Madden G, Symans M, Wongprasert N. Analytical and numerical study of a smart sliding base isolation system for seismic protection of buildings. Comput Aided Civ Infrastruct Eng 2003;18:19–30.
[7] Makris N. Rigidity–plasticity–viscosity: can electrorheological dampers protect base-isolated structures from near-source earthquakes. Earthq Eng Struct Dyn 1997;26:571–91.
[8] MATLAB. The Math Works, Inc., Natick, Massachusetts; 2000.
[9] Nagarajaiah S. Structural vibration damper with continuously variable stiffness. U.S. Patent 6098969; 2000.
[10] Nagarajaiah S, Mate D. Semi-active control of continuously variable stiffness system. In: Proc. 2nd world conference on struc. control, vol. 1. New York: Wiley; 1998. p. 397–405.
[11] Nagarajaiah S, Reinhorn AM, Constantinou MC. Nonlinear dynamic analysis of 3-D-base-isolated structures. J Struct Eng, ASCE 1991; 117(7):2035–54.
[12] Ramallo J, Johnson EA, Spencer B. Smart base isolation systems. J Eng Mech, ASCE 2002;128(10):1088–99.
[13] Sahasrabudhe S, Nagarajaiah S, Hard C. Experimental study of sliding isolated bridges with smart dampers subjected to near source ground motion. In: Proc. 13th engrg. mech. conference. CDROM. 2000.
[14] Singh M, Matheu E, Saurez L. Active and semiactive control of structures under seismic excitations. Earthq Eng Struct Dyn 1997;26: 193–213.
[15] Spencer BF, Johnson EA, C RJ. Smart isolation for seismic control. JSME Int J, Series C 2000;43(3):704–11.
[16] Spencer BF, Nagarajaiah S. State of the art of structural control. J Struct Eng, ASCE 2003;129(7):845–56.
[17] Symans MD, Kelly SW. Fuzzy logic control of bridge structures using intelligent semi-active seismic isolation. Earthq Eng Struct Dyn 1999; 28:37–60.
[18] Yang JN, Kim J, Agrawal A. Resetting semiactive stiffness damper for seismic response control. J Struct Eng, ASCE 2000;26:1427–33.
[19] Yang JN, Wu J, Reinhorn A, Li Z. Control of seismic-excited buildings using active variable stiffness systems. Eng Struct 1996;18(8): 589–96.
[20] Yashioka H, Ramallo JC, Spencer BJ. Smart base isolation strategies employing magnetorheological damper. J Struct Eng, ASCE 2002; 128(5):540–51.
[21] Yoshida K, Kang S, Kim T. LQG control and H_∞ control of vibration isolation of multi-degree-of-freedom systems. In: Proc. 1st world conf. on struc. control, vol. TP4. 1994. p. 43–52.
[22] Zhang Y, Iwan W. Protecting base-isolated structures from near-field ground motion by tuned interaction damper. J Eng Mech, ASCE 2002; 128(3):287–95.